



Magnetic/conductive composite fibre: A multifunctional strain sensor with magnetically driven property



Li Ding^a, Shouhu Xuan^{a,b,*}, Jiabin Feng^a, Xinglong Gong^{a,*}

^a CAS Key Laboratory of Mechanical Behavior and Design of Materials, Department of Modern Mechanics, University of Science and Technology of China (USTC), Hefei 230027, PR China
^b National Synchrotron Radiation Laboratory, USTC, Hefei 230027, PR China

ARTICLE INFO

Article history:

Received 16 February 2017
 Received in revised form 24 April 2017
 Accepted 28 April 2017
 Available online 8 May 2017

Keywords:

A. Fibres
 A. Smart materials
 B. Magnetic properties
 B. Electrical properties
 Multifunctional nanocomposite

ABSTRACT

Here reports a latex yarn-silver nanowires-magnetic polymer based magnetic-conductive composite fibre (MCF) prepared by a simple dropping-drying process. The magnetic-mechanic-electric coupling properties of the multifunctional fibre are systematically investigated. It's found that the electrical resistance increases by 44% when the tensile strain reaches 8%. Meanwhile, the relative resistance meets a dramatically variation by applying the external magnetic field. For instance, a 1.5% relative resistance increment is achieved by bending the MCF to 44 deg under a 400 mT magnetic field, in which the magnetic induced force is equivalent to 15 mN. Afterwards, a potential mechanism is proposed to investigate the magnetic-mechanic-electric coupling behavior. The results show that the MCF can be applied both as strain sensors and magnetic field sensors. Furthermore, a magnetic-sensing on-off switch and a flexible gripper are subsequently developed, demonstrating that the MCF possesses high potential in the implementation of intelligent soft sensors and actuators.

© 2017 Published by Elsevier Ltd.

1. Introduction

Multifunctional composites have been verified as an enticing candidate for various applications including wearable electronics and actuating devices. During the past decades, various efforts have been done to tailor novel multifunctional composites via tactfully integrating desirable properties such as physical, electrical, and mechanical properties, together. Multifunctional composites integrated by nanosized units usually exhibited unique characteristics such as electrical [1,2], magnetic [3,4], biological [5,6], optical [7,8], mechanical [9,10], and mechanical/electrical coupling properties [11,12]. As one of the most promising next-generation materials, multifunctional nanocomposites have exhibited great potential in sensing systems [13,14], soft robotics [15,16], biomedical therapy [5,8], energy storage [17,18], drug delivery [19,20], etc.

Typically, the mechanical/electrical coupling nanocomposites have been developed for strain sensor due to their strain dependent conductivity. Conductive fillers such as graphene, graphene oxide, carbon black, carbon nanotubes, metal nanoparticles, metallic nanowires, semiconducting nanowires were usually introduced

into the polymer matrix to form the hybrid sensing system [21–25]. Wei et al. reported that the resistivity of waterborne polyurethane conductive nanocomposites embedded with silver nanowires (AgNWs) and nano-SiO₂ decreased about 5000 times due to the hybrids nanostructure [24]. Lin et al. fabricated graphene-based elastomer with an effective segregated nanostructured graphene network. As a multifunctional stretchable sensing material, it possesses good sensitive reproducibility even the strain reached up to 60% [22]. Recently, the sensitive stretchable and durable strain sensors have attracted increasing interests due to their wide potential in health monitoring and motion capturing [26–28]. Till now, the easy-to-manufacture flexible strain sensors have become the most desirable candidate.

During the past decade, varieties of high-performance flexible sensors have been successfully constructed. Strain sensors with thin/bulk film structure, multilayer structure, fibrous structure, porous structure, and 3D geometry structure were developed for applications [1,11,12,24,29]. Among them, the fibrous structures are highly desirable [17,30,31] due to their flexibility, comfortableness, softness, and light weight. Recently, various fibre-based sensors and sensing networks have been assembled for electronic wearable systems including strain, pressure, chemistry, optics and humidity sensors [32–37] etc. Lee et al. fabricated highly stretchable conductive fibres composed of silver nanowires and silver nanoparticles embedded in a styrene-butadienestyrene

* Corresponding authors. CAS Key Laboratory of Mechanical Behavior and Design of Materials, Department of Modern Mechanics, University of Science and Technology of China (USTC), Hefei 230027, PR China (S. Xuan).

E-mail addresses: xuansh@ustc.edu.cn (S. Xuan), gongxl@ustc.edu.cn (X. Gong).

elastomeric matrix [32]. Qu et al. created hollow reduced graphene oxide/conducting polymer composite fibres and hollow bare reduced graphene oxide fibres with good flexibility and electrical conductivity [17].

Moreover, magnetic nanocomposites are widely applied in artificial muscle, dampers, robotics and drug delivery because of their easy controllability, non-contact actuation and quick response [15,16,38]. Recently, researches on the combination of magnetism and other functions have drawn increasing attention [32,35–37]. Nguyen et al. added silicone and graphite into magnetic polymer actuation to achieve the self-sensing performance [15]. Wei et al. designed an intelligent flowerlike platform which could be controlled with external magnetic field [16]. More important, the magnetically dependent conductivity enables the hybrid materials to be applied as magnetic field sensors. For example, Mietta et al. dispersed silver-covered magnetite particles ($\text{Fe}_3\text{O}_4@\text{Ag}$) within polydimethylsiloxane (PDMS) to fabricate a magnetic field sensor. Typically, the electrical resistance of the sensor decreased monotonically with the applied magnetic field (negative magnetoresistance). By combining the carbon nanotube (CNT) with sponge skeleton, Ge et al. developed a novel magnetorheological elastomer which could be applied as a magnetic field sensor [39]. Obviously, the magnetic/conductive coupling composite will be favorable for both strain and magnetic field sensor, while it also possesses the magnetically driven characteristics. In consideration of the facility of the fibre-like structure, the magnetic-conductive composite fibres are important for not only the fundamental studies but also the practical applications.

In this work, a novel coaxial composite fibre with both sensing and magnetically driven properties is fabricated via a simple dropping-drying process. The composite is based on intertwined excellent flexible and stretchable lastex yarn with helical AgNWs network as conductive core and magnetic polymer as the protective shell. The electrical and mechanical properties under tensile and flexuous conditions are systematically investigated. The composite fibres exhibits ideal flexibility, large deformation, appropriate elasticity and sensing properties, which possesses high potential in tensile and bending sensor. Specially, their deformation and electrical resistance could be changed by magnetic field, demonstrating that they can be also applied as magnetic field sensor. Moreover, the influencing factors of electrical conductivity are systematically analyzed and a possible mechanism is proposed. Finally, a magnetic on-off switch and a gripper based on the composite fibres are developed.

2. Experiment section

2.1. Materials

Lastex yarns (outer diameter of about 0.5 mm) were supplied from Danyang Elastic Yarn Factory, China. Reagents (analytical grade purity) for fabrication of AgNWs were purchased from Sino-pharm Chemical Reagent Co. Ltd., Shanghai, China and were used without further purification. The PDMS precursor and curing agent (Sylgard 184) were purchased from Dow Corning GmbH, USA. The carbonyl iron particles (CIPs) with an average diameter of 7 μm were purchased by BASF in Germany.

2.2. Fabrication of magnetic-conductive composite fibre

The lastex yarn (LY) was immersed into the mixed solution of 100 mL ethanol and 1 mL 3-Triethocysilylpropylamine (APTES) for 24 h. After that, the treated lastex yarn was fixed perpendicular to the ground and stretched to 150% of the tensile strain. Then it was coated with AgNWs dispersion (fabricated by a facile synthetic

method [40]) and dried in the air for 30 s. The intermolecular hydrogen bonds form between >C=O of polyvinyl pyrrolidone (PVP) on the surface of AgNWs and —NH_2 of APTES on the surface of lastex yarn, which can help to immobilize AgNWs on the surface of lastex yarn tightly. This coating operation was repeated for several times to form an AgNWs network within the lastex yarn. After the above dropping-drying process, a stretchable conductive fibre based on helical AgNWs networks was obtained (defined as Ag shell, LY@Ag). Finally, another shell material, PDMS/CIPs, was synthesized by mixing CIPs with PDMS (PDMS curing ratio of 10:1, CIPs and PDMS mass ratio of 2:3). The magnetic polymer precursor (liquid PDMS/CIPs) was also coated onto the surface of LY@Ag by the dropping-drying process. After being dried in a hot plate for 30 min (90 °C), the magnetic-conductive composite fibre (MCF, LY@Ag@PDMS/CIPs) was obtained.

In addition, the mass fractions of AgNWs in MCFs were maintained at 0.15, 0.20, 0.25, 0.30, and 0.35 wt%, respectively. For convenience, MCFs with different mass fractions of AgNWs were defined as X wt% MCF, where X was the mass fraction of AgNWs.

2.3. Characterization

The microstructures of LY, LY@Ag, LY@Ag@PDMS/CIPs were characterized by scanning electron microscopy (SEM, Sirion 200). The rheological properties of PDMS/CIPs were measured by a rheometer (Physica MCR 301, Anton Paar Co., Austria) with a parallel rotor. Magnetic flux density ranged from 0 mT to 960 mT was achieved by adjusting the electromagnetic coil current from 0 A to 4 A. The test was undertaken in shear oscillation mode at 25 °C. The tensile properties of the samples were tested with the Material Test System (MTS) (MTS criterion 43, MTS System Co., America) and a dynamic mechanical analyzer (DMA, Q800, TA). Modulab® material test system (Solartron analytical, AMETEK advanced measurement technology, Inc., United Kingdom) was used to measure the electrical properties. Magnetic field in flexuous tests was afforded by commercial permanents or Magnetic Power System (IGLF-150, Beijing saidi new electromechanical technology Co., China).

3. Results and discussion

3.1. Structural characterization of the MCFs

Fig. 1a schematically illustrates the fabrication processes of the magnetic-conductive composite fibre. The procedure involves three main steps: (i) the modification of commercial lastex yarn, in which the inner spandex fibre is the core and acrylic fibre is helically wound around their surface, (ii) coating of the lastex yarn with AgNWs, (iii) coating of the LY@Ag with magnetic polymer (PDMS/CIPs). For simplicity, the final LY@Ag@PDMS/CIPs product is named as MCF (magnetic-conductive composite fibre). The scanning electron microscopy images of MCF are shown in Fig. 1b and 1c, which exhibit the coaxial structure and the close contacted interface between acrylic fibres and PDMS/CIPs. The final MCF shows the clear core@shell@shell coaxial structure, with the spandex fibres inner core, the helical AgNWs network and acrylic fibres middle shell, and the PDMS/CIPs outer shell. The tight connection between LY@Ag and PDMS/CIPs guarantees MCF's stable mechanical properties under various kinds of excitations (including large deformation loading). The MCF can be stretched to 100% of tensile strain (Fig. 1d) and bent into various shapes (Fig. 1e), which shows the excellent stretchability and flexibility. Fig. 1f shows that MCFs can be mass-produced because of its convenient manufacturing process.

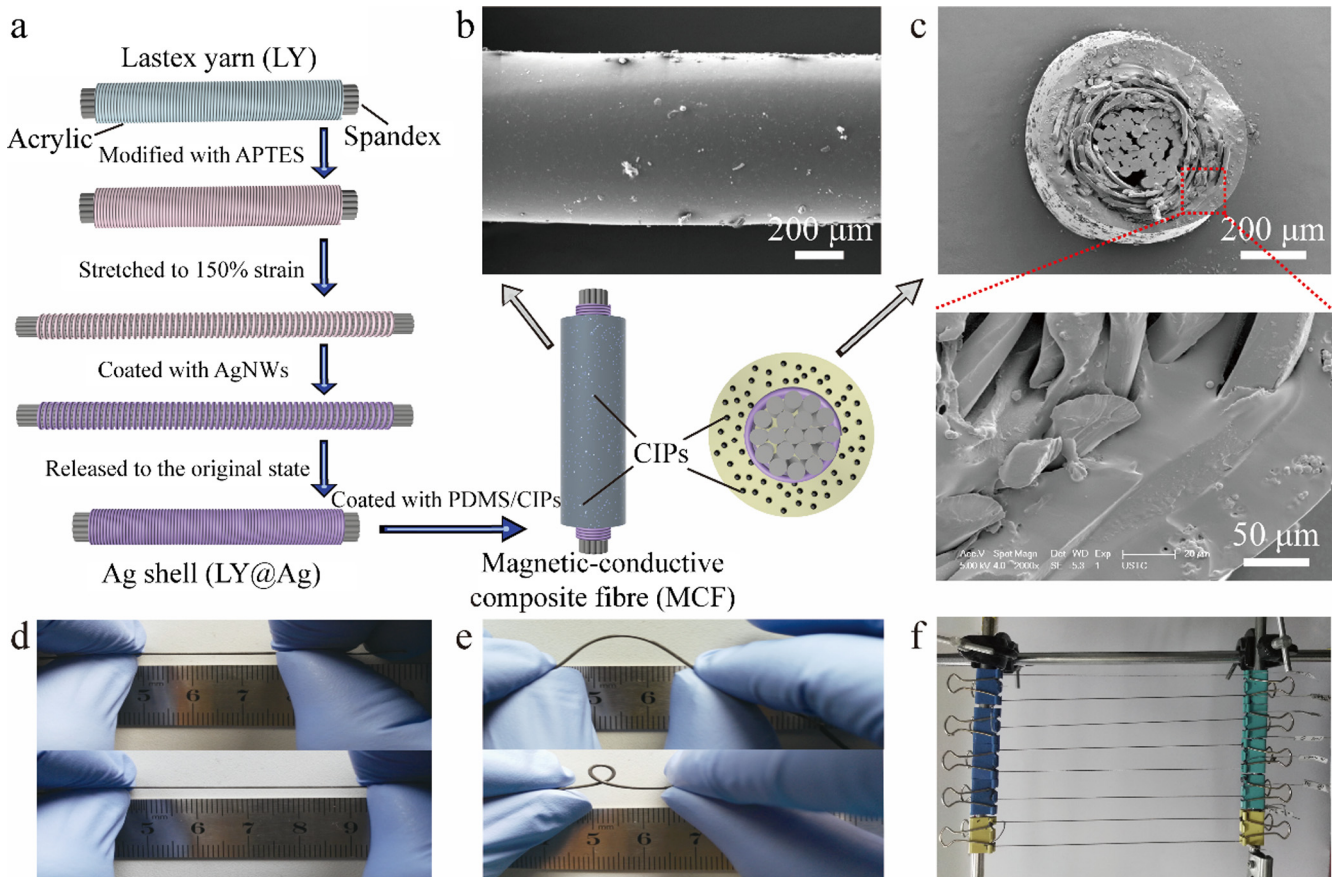


Fig. 1. (a) Schematic illustration for fabrication process of MCF. (b) SEM image of MCF. (c) SEM images of the cross section of MCF. (d) Optical images of the original and stretched MCF. (e) Optical images of MCF being deformed into different shapes. (f) A photograph of the fabrication process.

The SEM images of chemically modified LY, LY@Ag and MCF are shown in Fig. 2a, c and e, respectively. The pristine LY exhibits the typical core/helical shell structure (Fig. 2b), which is comprised of a bundle of elastic spandex fibres and the helical acrylic fibres skin. After the immobilization of the AgNWs, the surface of acrylic fibres in the LY becomes rather rough (Fig. 2d). The inset shows that AgNWs are well adhered to the acrylic fibres (Fig. S1). After the further coating with PDMS/CIPs, the AgNWs are completely sealed by

the magnetic polymer, which can prevent their falling off under the external stimuli (Fig. 2e, f and S2–4). Here, the density of AgNWs network and thickness of PDMS/CIPs can be controlled in the dropping-drying process (Fig. S5 and S6).

PDMS/CIPs and MCF present unique magnetic properties since CIPs are the soft magnetic material whose magnetic remanence and coercivity are very low. Fig. 3a shows the hysteresis loops of PDMS/CIPs and MCF. The saturation magnetization (M_s) of

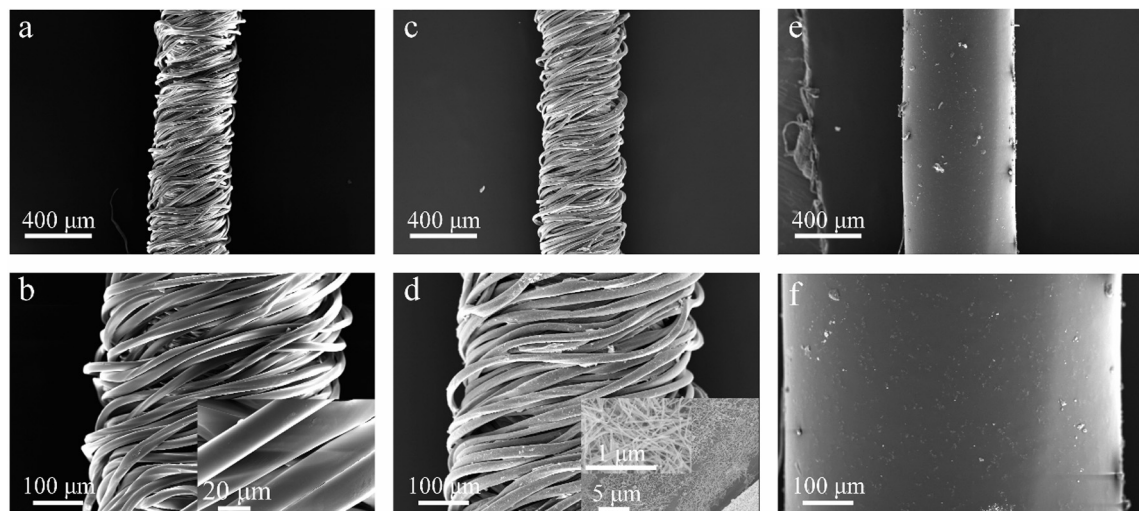


Fig. 2. SEM images with different magnifications of the chemically-modified LY (a and b), LY@Ag (c and d) and MCF (LY@Ag@PDMS/CIPs) (e and f), respectively.

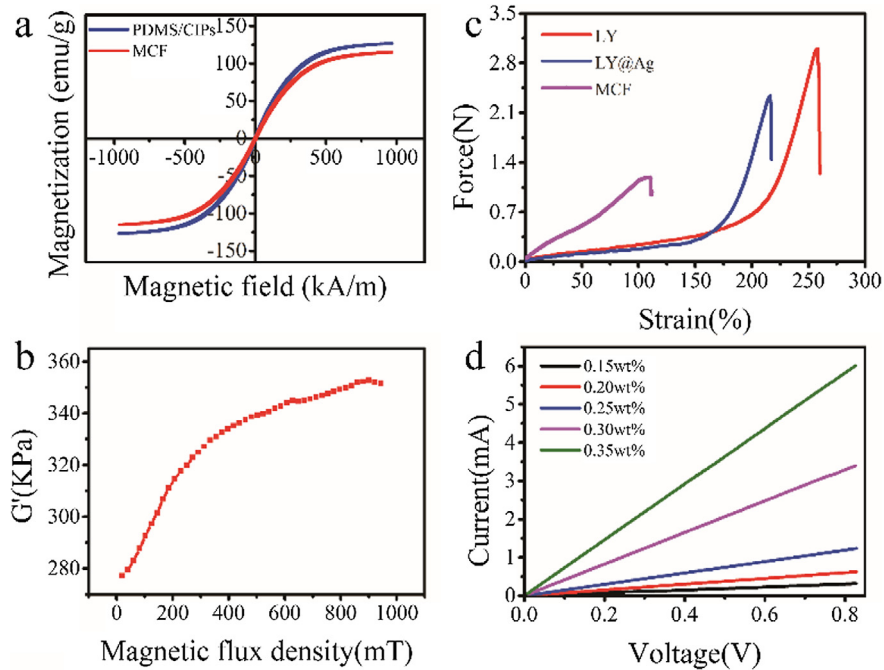


Fig. 3. (a) Vibrating sample magnetometer (VSM) data for PDMS/CIPs and MCF. (b) Dynamic storage modulus of PDMS/CIPs under various magnetic flux densities. (c) Tensile strength-strain curves for LY, LY@Ag and MCF. (d) I–V curves of MCFs with different mass fraction of AgNWs.

PDMS/CIPs and MCF are 126.83 emu/g and 115.03 emu/g, respectively. The lower M_s of MCF is attributed to the smaller mass fraction of CIPs in MCF than that in PDMS/CIPs. Additionally, the residual magnetization and coercivity of PDMS/CIPs and MCF are 3.14 emu/g, 2.44 emu/g and 6.66 kA/m, 6.50 kA/m, respectively, showing an ideal and quick magnetic response performance. Due to the presence of the CIPs, the PDMS/CIPs and MCF are magnetorheological materials, whose storage modulus can increase under applying the magnetic field [41–44]. The CIPs can be saturated under 750 kA/m magnetic field, thus both the PDMS/CIPs and MCF can reach to a large storage modulus when a relatively small magnetic field is applied. Here, the storage modulus of PDMS/CIPs increases with magnetic flux density and it can reach to as high as 350 kPa (Fig. 3b). Similarly, the MCF exhibits the typical magnetorheological behavior. Due to the fibrous structure of the MCF, it is very difficult to test the magnetorheological effect under our present instrument.

Due to the unique hierarchical structure of lastex yarn, the stress would be mainly focused on the inner spandex fibres other than the acrylic fibres when the lastex yarn is stretched in a certain strain range. As shown in Fig. 3c, the force-strain curves of LY@Ag and LY are similar and exhibit linear characteristic when the strain is smaller than 150%. The first damaging strain and corresponding tensile force of LY and LY@Ag are 258%, 216% and 3.00 N, 2.34 N, respectively. Moreover, the tensile force is 0.94 N while LY is applied to 216%, indicating that AgNWs network reduces the flexibility and increases the elastic modulus when applied strain >150%. Additionally, when 100% strain is applied, the force of MCF is 1.14 N, about four times larger than that of LY or LY@Ag, demonstrating that MCF is more robust. Similarly, the tensile force of MCF is proportional to the strain.

Due to the presence of AgNWs, the MCFs are conductive and their conductivities are dependent on mass fraction of AgNWs. It is observed that a linear relationship between the current and voltage of the specimens (Fig. 3d). Moreover, it is calculated from the linear I–V curves that the resistivity of MCFs with 0.15 wt%, 0.20 wt%, 0.25 wt%, 0.30 wt%, and 0.35 wt% AgNWs, are

$4.3 \times 10^{-2} \Omega \text{ m}$, $2.1 \times 10^{-2} \Omega \text{ m}$, $1.1 \times 10^{-2} \Omega \text{ m}$, $4 \times 10^{-3} \Omega \text{ m}$, and $2.3 \times 10^{-3} \Omega \text{ m}$, respectively, indicating the decreasing trend with increasing of the AgNWs weight fraction. Consequently, it is highlighted that the density of AgNWs network determines electrical conductivity of MCF. In conclusion, the final MCF possesses appropriate toughness, linear elasticity, good electrical performance as well as magnetically driven property. More importantly, the conductivity of the MCF is highly dependent on the external applied stress/strain and magnetic field, thus it possesses high potential in force sensor or magnetic field sensor.

3.2. Tensile strain responsive properties of the MCFs

The conductivity of MCFs is highly dependent on the dispersing state of AgNWs, therefore, the MCF can be employed as a tensile strain sensor due to the AgNWs networks varied under the stress. Here, the two ends of magnetic-conductive composite fibre were mounted with Cu electrodes by using conductive silver paste. Then, the electromechanical properties of the MCF tensile strain sensor under different stress can be studied. We measure the normalized resistance change $\Delta R = (R' - R)/R$, where R' and R are the electrical resistances at strain and initial state, respectively, in synchrony with the tensile strain of the sensor. In this work, the 0.2 wt% AgNWs MCF tensile strain sensor is selected to be tested and the relative resistance and tensile force variations are measured with the strain varied from 1% to 8% (Fig. 4a and b). It is observed that the relative resistance increases about 43.6% when the strain is 8%. Additionally, the MCF tensile strain sensor exhibits a linear dependency on the applied strain. The stability of the MCF tensile strain sensor is further evaluated by periodic stretch and release cycles. More details of electrical properties with different tensile strain are shown in (supporting information (Figs. S7 and S8)). Under applying 10% strain on the 0.35 wt% MCF tensile strain sensor, the relative resistance is nearly kept as a constant at 12% after 80 cycles, demonstrating the excellent stability (Fig. 4c). Additionally, the relative resistance variation presents good linear relation-

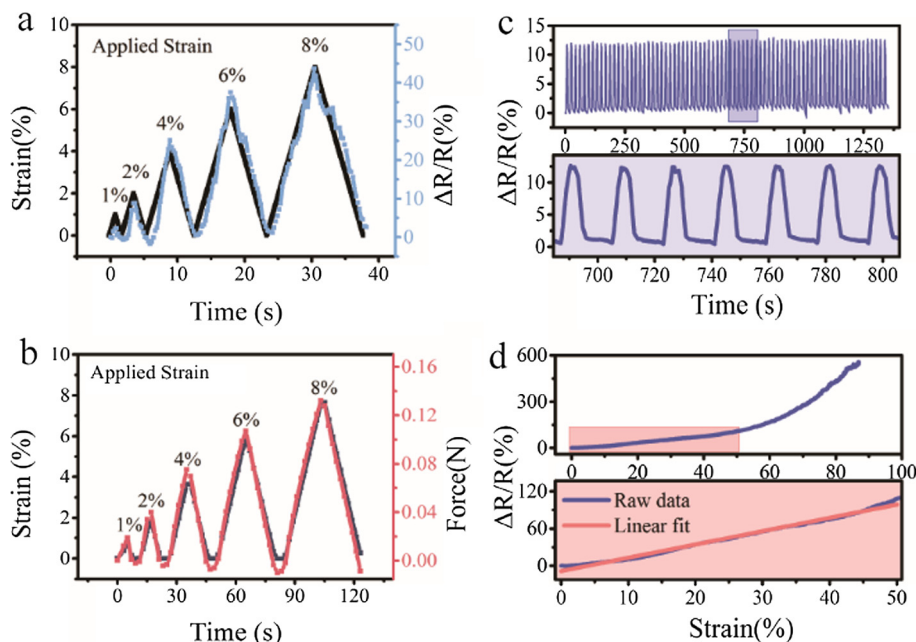


Fig. 4. (a) Relative resistance variation under gradually increasing step strain from 1% to 8% strain. (b) Tensile force variation of the sensor under gradually increasing step strain from 1% to 8% strain. (c) Change in the resistance with no strain and 10% applied strain during 80 stretch-release cycles. Insets: Close-up of the selected areas. (d) Curve for the relative resistance changing with the strain. The inset shows the linear-change part.

ships with the tensile strain (Figs. 3c and 4d), which has the linearity of $R^2 = 0.997$ for the fitting curve. MCF tensile strain sensor also had good sensitivity. With the strain varying from 0 to 50%, the relative resistance of 0.25 wt% MCF tensile strain sensor changed about 100%. In summary, the electrical and mechanical properties of MCF tensile strain sensor showed good sensitivity, linearity and stability in tensile tests (Fig. S9).

3.3. Flexuous deformation responsive properties of the MCFs

As the relative resistance of the present composite fibre is dependent on the bending angle, MCF can be also used as a bending sensor. The MCF is fixed onto a plastic film substrate and the electrical properties are measured under manual bending tests (Fig. S10). Fig. 5a shows the relative resistance variation as a function of bending angle, which is defined as the central angle corresponding to the arc length. The $\Delta R/R$ increases from 0 to 3.56% along with the bending angle varies from 0° to 180° . In addition, the MCF bending sensor has a 3% increment in resistance from 0° to 150° (Fig. 5b) and shows good mechanical stability and repeatability for at least five cycles. The electrical responses are

maintained well for different bending angles and are reproducible under multiple tests. Consequently, the MCF is a potential bending sensor.

In comparison to the previously reported strain sensors based on flexible polymer, MCF sensors are not limited by the weak adhesion of conductive materials and the buckling/wrinkling of the film [45]. Compared with the fully encapsulated sensors, MCF sensors have higher softness, higher flexibility and smaller size. Therefore, they are easier to be mounted on the skin and attached to complex surfaces. Furthermore, most sensors with desirable properties (i.e., high sensitivity) are only single functional whereas MCFs have demonstrated various of promising applications, which will be shown as the following.

3.4. Magnetic responsive performance of the MCFs

Due to the magnetic characteristic, the MCF also can be used as a low-cost portable magnetic field sensor (Fig. 3). The influence of the magnetic field on the relative resistance is investigated in two different ways. In the first method, with one end being fixed like a cantilever beam, MCF is subject to magnetic field force. Here, the

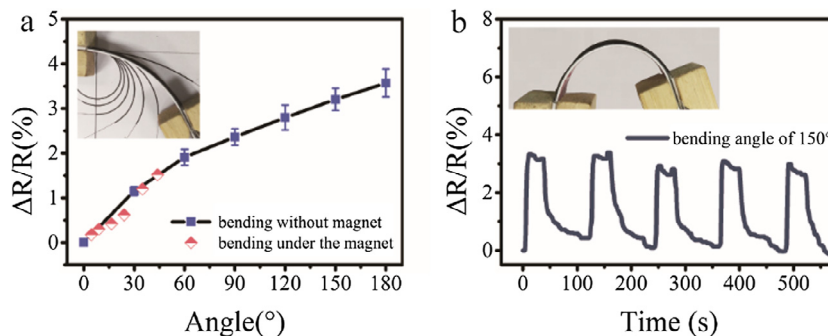


Fig. 5. (a) Relative resistance variation along with the change of bending angle (red points will be mentioned in Section 3.4). Inset: the digital photograph of bending tests. (b) Relative resistance variation during cyclic bend-relax deformation at 150° . (For interpretation of the references to colour in this figure legend, the reader is referred to the web version of this article.)

MCF is fixed on a conventional 0.1 mm thick plastic film with both ends glued by conductive tapes, and then it is clamped by a small aluminum fixture (Fig. 6a and S12). Fig. 6b indicates that the relative resistance increases obviously with magnetic flux density from 150 mT to 400 mT. The larger the magnetic field strength, the stronger the magnetic force and the bigger the deformation. Additionally, the peak value of relative resistance variation keeps at around 1.2% during cycling loadings of 350 mT magnetic field, thus demonstrating the good electrical property and mechanical deformation stability (Fig. 6c).

The weight loading tests are carried out to investigate the influence of mechanical force on magnetic field sensor (Fig. 6d and S12b). The beam-end deflections at different loaded weights are measured, thus the force-deflection fitting curve is obtained. The equivalent force under magnetic field is evaluated via interpolating the foregoing testing data under magnetic field into the fitting curve (Fig. 6e). Afterwards, the corresponding bending angles of the cantilever beam structure under magnetic field are analyzed. Fig. 6f depicts the curves of bending angle-magnetic field and equivalent force-magnetic field. Here, the influence of the magnetic field force can be estimated by calculating the equivalent force through the loading weights test (Fig. 6f).

The second testing method for the magnetic sensor is depicted in Fig. 6g. With both ends being fixed, magnetic field sensor arched like invertebrates crawling under the magnetic field afforded by a permanent magnet. The difference of relative resistance changes under different magnetic field is clearly distinguished (Fig. 6h). The resistance variation under the 240 mT magnetic field is 7.6%, about 4.5 times of that under 80 mT. And the deformation and the resistance variation of magnetic field sensor exhibit considerable stability under the same magnetic field strength (Fig. 6i). Unfortunately, the hysteresis behavior appears due to the inherent hysteresis associated with magnetic loading.

In comparison to the previously reported microfiber/ferrofluid-assisted magnetic field sensors [46,47], the preparation of the MCF sensors are very easy to manufacture and the sensitivity is good. Therefore, they are attractive in the future applications.

3.5. Sensing mechanism of the MCFs

The sensing properties of MCF sensors are essentially based on the microstructure change of AgNWs network. Apparently, the total resistance of MCF (R) consists of the contact resistance of AgNWs joints (R_c) and their inherent resistance (R_w). When the

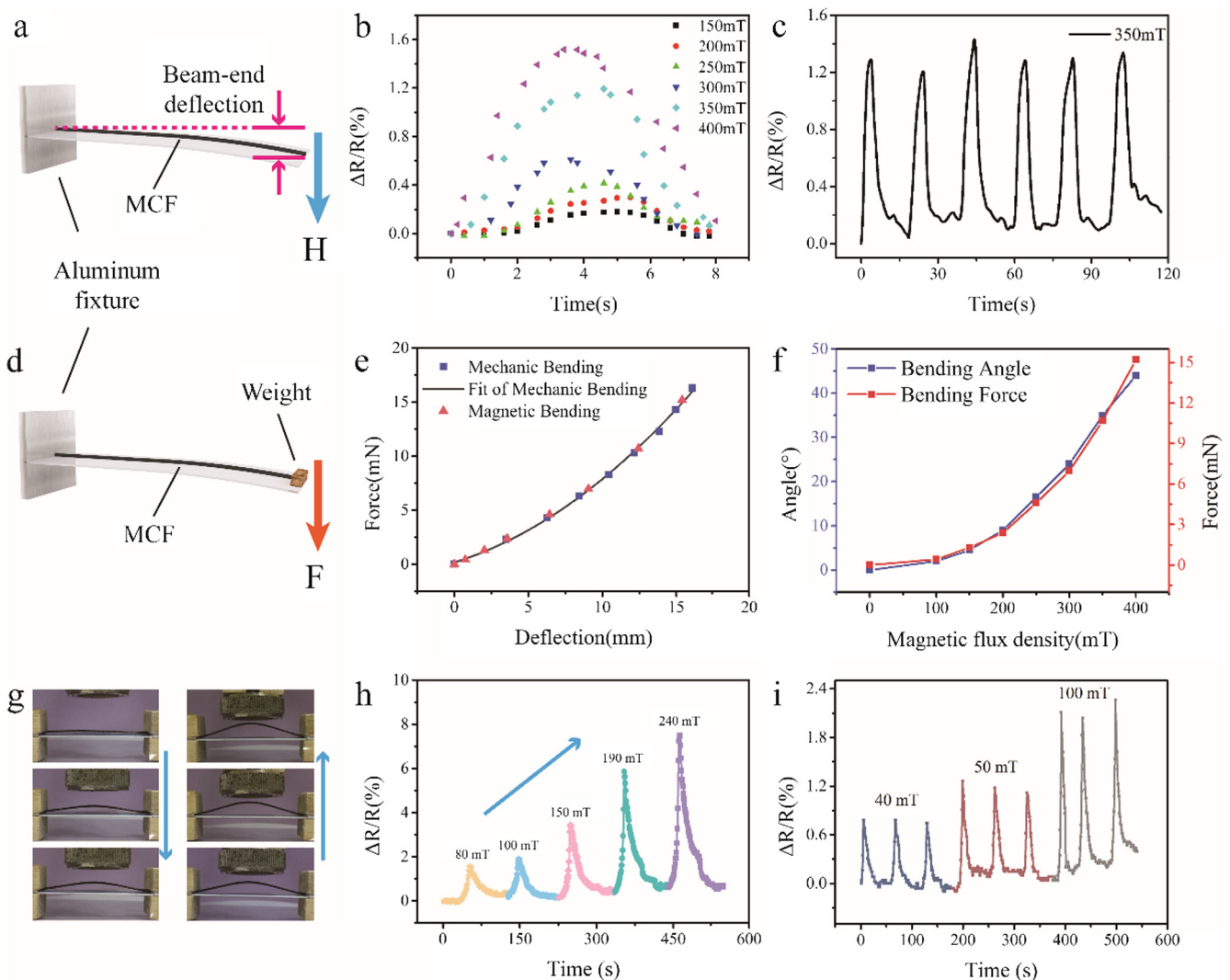


Fig. 6. (a) The schematic illustration of magnetic field sensor as a cantilever beam under magnetic field. (b) Relative resistance variation of the fibre under different magnetic strength. (c) Relative resistance variation at 350 mT for several cycles. (d) The schematic illustration of MCF in weight loading test. (e) The force-deflection fitting curve. (f) The bending angle-magnet curve and bending force-magnetic flux density curve. (g) Optical images of MCF with both ends fixed under different magnetic field. (h) Relative resistance variation with magnetic strength increasing from 80 mT to 240 mT. (i) Relative resistance variation from 40 to 100 mT for three cycles.

strain is applied, the AgNWs embedded in the magnetic polymer are stretched and slide. Simultaneously, the number of AgNWs joints decreases and the distance between NWs (d , defined as the distance between the mid-points of adjacent NWs) increases, resulting in the growth of the resistance generated by the applied strain (Fig. 7a). The contact resistance can be approximately estimated as

$$R'_c = Cd' = Cd(1 + \varepsilon) = R_c(1 + \varepsilon) \quad (1)$$

where C is a constant related to the contact state between the AgNWs network, ε is the applied strain, d' and R'_c are the distance between AgNWs and the contact resistance at a strain of ε respectively. Another influencing factor of the resistance is the change of the length of the AgNWs. According to the law of resistance, the inherent resistance can be described as

$$R'_w = \rho_{Ag} \frac{l'}{A} = \rho_{Ag} \frac{(1 + B\varepsilon)l}{A} = R_w(1 + B\varepsilon) \quad (2)$$

where ρ_{Ag} is the silver resistivity, l' and l are the length of the AgNWs at the tensile state and the initial state respectively, A is the cross-sectional area of the AgNWs (as a constant under small strain), R'_w is the inherent resistance at strain of ε , B is a constant related to the orientational distribution of the AgNWs (the angle to the stretching direction, such as vertical or parallel to the stretching direction). Obviously, $B < 1$. Therefore, the relative resistance variation at strain of ε can be determined as

$$\frac{\Delta R}{R} = \frac{R' - R}{R} = \frac{(R'_c + R'_w) - (R_c + R_w)}{R_c + R_w} = \frac{(R_c + BR_w)\varepsilon}{R_c + R_w} \quad (3)$$

It is quite clear that $\Delta R/R$ is nearly proportional to ε , which is consistent with the response curve of MCF tensile sensor. However, when a large strain is applied, the distance between AgNWs exceeds the threshold value, and some joints disconnect, resulting in the remarkable increase in the resistance.

To better explain the mechanism for relative resistance variation, the total resistance R of MCF can be considered as two parts of equivalent resistance R_0 in parallel, which are bisected along with neutral surface. Therefore, R can be calculated as $R = R_0/2$. When stretched or bent, both sides of the neutral surface are stretched, resulting in the increase of resistance. According to the theorem of parallel circuit, the resistance of tensile sensor should

be described as $R' = (R_0 + R_1)/2$. And the resistance of bending sensor R' , can be depicted as

$$R' = \frac{(R_0 + R_2)(R_0 + R_3)}{(R_0 + R_2 + R_0 + R_3)}, \text{ whereby, } R_2 > R_3 \quad (4)$$

where R_2 is the increasing resistance of outer half part, R_3 is the increasing resistance of inner half part (Fig. 7b).

Under the magnetic field force, the MCFs are considered to be a tensile/bending hybrid sensor. The total resistance variation comes from both bending and stretching. For the magnetic field sensor with one end fixed, the results are similar to those of bending sensor (Fig. 5a), demonstrating the magnetic field sensor with one end fixed can be essentially considered to be a bending sensor. That is also why the bending angles are adopted to characterize the deformation of magnetic field sensor. When both ends of MCF are fixed, the magnetic force not only bends but also stretches the MCF. In comparison to the influence of tension, the effect of flexion is too smaller to be ignored, thus the relative resistance variations can be considered to be fully caused by the tension. Therefore, under applying the external magnetic field, the MCF should be roughly taken as tensile sensor instead of bending sensor.

3.6. Other applications such as MCF-based smart switch and gripper

MCF exhibits good stretchability, flexibility as well as mechanical properties. It attracted extraordinary interesting because its electrical-mechanical coupling behavior can be easily controlled by an external magnetic field. The magnetic materials can be greatly influenced by the external magnetic field, particularly under non-contact conditions [48]. Hereby, a magnetism-sensing switch which is able to work in a confined space is fabricated by the MCF. Fig. 8a shows the schematic illustration of the electric circuit of the magnetism-sensing switch system. When the magnet is close to the glass tube, the magnetism-sensing switch in the tube is contacted with the metal electrode to connect the circuit (the relevant lamp is lit). Afterward, when the magnet is moved away, the switch separates away immediately and the circuit is disconnected (Fig. 8b). By controlling the external magnetic field, the magnetism-sensing switch is able to be turned on and off (Movie S1).

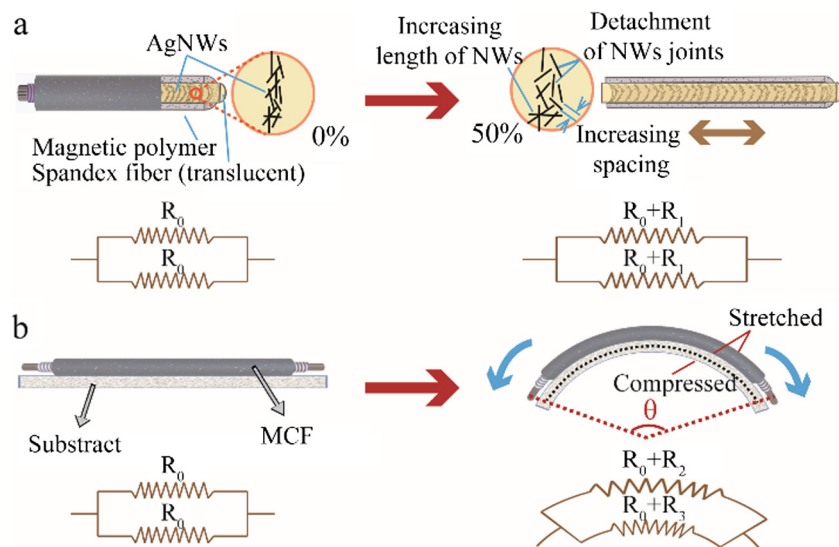


Fig. 7. (a) Schematic illustrations of the MCF tensile sensing mechanism and the accompanying circuit variations. (b) Schematic illustrations of the MCF bending sensing mechanism and the accompanying circuit variations.

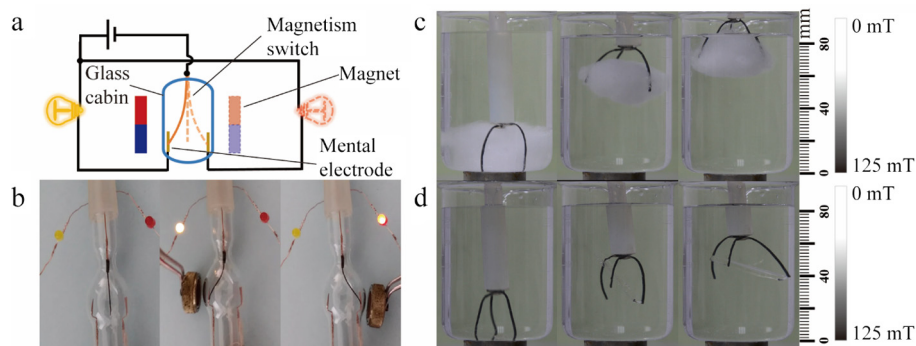


Fig. 8. (a) The schematic illustration and (b) the working process of magnetism-sensing switch. (c) Demonstration of MCFs assembled as a gripper to transport soft cotton ball and (d) irregular PDMS plate (the magnet is fixed under the breaker).

Moreover, the MCFs can also be used as a flexible gripper. For flexible grippers based on whether shape memory alloys or pneumatic elastomers, the complex manufacturing/operation and bulky dimensions are two major limitations [49,50]. Nevertheless, these two restrictions were resolved in the MCF gripper. We fixed three MCFs (2 cm in length and 0.07 g in weight) on the PVC rod to fabricate a triangular gripper. The gripper arms would bend to the field direction with a certain holding force under the external magnet. Fig. 8c and 8d represent the entire process (gripping, catching up and moving) of manipulating different objects from the bottom to the top of the water filled container (Movie S2–5). The transport height and the corresponding approximate magnetic field density are marked in graphs, respectively. The first object is a cotton ball (4 cm in diameter) and the other one is a PDMS plate with irregular surface (5.0 mm in thickness and 2.0 g in weight). Owing to the super flexibility and deformability of the composite fibre, the gripper can adaptively change its shape to grab the cotton ball and a flat object with irregular shape without damaging the surface texture of the material, which must be responded for the super flexibility and deformability of the MCF. Due to the protection of outer PDMS layer, the composite has good acid resistance and heat resistance [16]. Also, this triangular gripper with alterable shape and simple actuating system (a stick support and an external magnet merely) can be widely used in some special conditions, for example, going through the channel with a smaller operation space. Ulteriorly, the devices can realize the real-time motion detection, which can be applied to get the extent of its stretching or bending and determine the next operations for pre-judgment.

4. Conclusions

In summary, we developed a multifunctional MCF sensor by combining commercial lastex yarn, AgNWs and PDMS/CIPs into a coaxial structure. Typically, the MCFs demonstrate exceptional electrical and mechanical properties with excellent flexibility and elasticity, providing the realization of tensile strain, bending deformation, and magnetic field sensing. As a tensile strain sensor, its relative resistance changes linearly with strain in the range of 50% and keeps very good stability and repeatability. The variation of the electric properties is distinctly dependent on the bending angle indicating that it can be employed as a bending sensor. Notably, due to the magnetic characteristic, the multifunctional MCF sensor can detect the magnetic field via monitoring the relative resistance change and thus can be applied in diverse smart sensing or actuating applications. Available applications such as magnetic switch and gripper are also developed to verify the active actuating property. Therefore, we believe that the design concept for such multifunctional composite can be extended to fabricate other com-

posites with integrated and enhanced properties towards various advanced applications, such as electronics system and soft actuators.

Acknowledgments

Financial supports from the National Natural Science Foundation of China (Grant Nos. 11572310, 11572309), the Strategic Priority Research Program of the Chinese Academy of Sciences (Grant No. XDB22040502), and the fundamental research funds for the Central Universities (WK2480000002) are gratefully acknowledged. This work is also supported by the Collaborative Innovation Center of Suzhou Nano Science and Technology.

Appendix A. Supplementary material

Supplementary data associated with this article can be found, in the online version, at <http://dx.doi.org/10.1016/j.compositesa.2017.04.025>.

References

- [1] Costa P, Silva J, Anson-Casas A, Martinez MT, Abad MJ, Viana J, et al. Effect of carbon nanotube type and functionalization on the electrical, thermal, mechanical and electromechanical properties of carbon nanotube/styrene-butadiene-styrene composites for large strain sensor applications. *Compos Part B Eng* 2014;61:136–46.
- [2] Wang S, Xuan S, Jiang W, Jiang W, Yan L, Mao Y, et al. Rate-dependent and self-healing conductive shear stiffening nanocomposite: a novel safe-guarding material with force sensitivity. *J Mater Chem A* 2015;3(39):19790–9.
- [3] Lazarus N, Meyer CD, Bedair SS, Slipper GA, Kierzewski IM. Magnetic elastomers for stretchable inductors. *ACS Appl Mat Inter* 2015;7(19):10080–4.
- [4] Li W, Liu Y, Leng J. Selectively actuated multi-shape memory effect of a polymer multicomposite. *J Mater Chem A* 2015;3(48):24532–9.
- [5] Shi X, Gong H, Li Y, Wang C, Cheng L, Liu Z. Graphene-based magnetic plasmonic nanocomposite for dual bioimaging and photothermal therapy. *Biomaterials* 2013;34(20):4786–93.
- [6] Colombo M, Carregal-Romero S, Casula MF, Gutiérrez L, Morales MP, Böhm IB, et al. Biological applications of magnetic nanoparticles. *Chem Soc Rev* 2012;41(11):4306–34.
- [7] Wang Y, Li B, Zhang L, Song H. Multifunctional mesoporous nanocomposites with magnetic, optical, and sensing features: synthesis, characterization, and their oxygen-sensing performance. *Langmuir* 2013;29(4):1273–9.
- [8] Majewski PW, Gopinadhan M, Osuji CO. Magnetic field alignment of block copolymers and polymer nanocomposites: scalable microstructure control in functional soft materials. *J Polym Sci, Part B: Polym Phys* 2012;50(1):2–8.
- [9] Han B, Sun S, Ding S, Zhang L, Yu X, Ou J. Review of nanocarbon-engineered multifunctional cementitious composites. *Compos Part A Appl S* 2015;70:69–81.
- [10] Tang G, Jiang Z-G, Li X, Zhang H-B, Hong S, Yu Z-Z. Electrically conductive rubbery epoxy/diamine-functionalized graphene nanocomposites with improved mechanical properties. *Compos Part B Eng* 2014;67:564–70.
- [11] Saw L, Mariatti M, Azura A, Azizan A, Kim JK. Transparent, electrically conductive, and flexible films made from multiwalled carbon nanotube/epoxy composites. *Compos Part B Eng* 2012;43(8):2973–9.

- [12] Ge J, Yao HB, Wang X, Ye YD, Wang JL, Wu ZY, et al. Stretchable conductors based on silver nanowires: improved performance through a binary network design. *Angew Chem Int Ed* 2013;125(6):1698–703.
- [13] Langley D, Giusti G, Mayousse C, Celle C, Bellet D, Simonato J-P. Flexible transparent conductive materials based on silver nanowire networks: a review. *Nanotechnology* 2013;24(45):452001.
- [14] Lee J, Kwon H, Seo J, Shin S, Koo JH, Pang C, et al. Conductive fiber-based ultrasensitive textile pressure sensor for wearable electronics. *Adv Mater* 2015;27(15):2433–9.
- [15] Nguyen VQ, Ahmed AS, Ramanujan RV. Morphing soft magnetic composites. *Adv Mater* 2012;24(30):4041–54.
- [16] Gao W, Wang L, Wang X, Liu H. Magnetic driving flowerlike soft platform: biomimetic fabrication and external regulation. *ACS Appl Mat Inter* 2016;8(22):14182–9.
- [17] Qu G, Cheng J, Li X, Yuan D, Chen P, Chen X, et al. A fiber supercapacitor with high energy density based on hollow graphene/conducting polymer fiber electrode. *Adv Mater* 2016;28(19):3646–52.
- [18] Zhong J, Zhang Y, Zhong Q, Hu Q, Hu B, Wang ZL, et al. Fiber-based generator for wearable electronics and mobile medication. *ACS Nano* 2014;8(6):6273–80.
- [19] Lum GZ, Ye Z, Dong X, Marvi H, Erin O, Hu W, et al. Shape-programmable magnetic soft matter. *PNAS* 2016;201608193.
- [20] Giltinan J, Diller E, Sitti M. Programmable assembly of heterogeneous microparts by an untethered mobile capillary microgripper. *Lab Chip* 2016;16(22):4445–57.
- [21] Ge J, Sun L, Zhang FR, Zhang Y, Shi LA, Zhao HY, et al. A Stretchable electronic fabric artificial skin with pressure-, lateral strain-, and flexion-sensitive properties. *Adv Mater* 2015.
- [22] Lin Y, Dong X, Liu S, Chen S, Wei Y, Liu L. Graphene-elastomer composites with segregated nanostructured network for liquid and strain sensing application. *ACS Appl Mat Inter* 2016;8(36):24143–51.
- [23] Wei Y, Chen S, Li F, Lin Y, Zhang Y, Liu L. Highly stable and sensitive paper-based bending sensor using silver nanowires/layered double hydroxides hybrids. *ACS Appl Mat Inter* 2015;7(26):14182–91.
- [24] Wei Y, Chen S, Li F, Liu K, Liu L. Hybrids of silver nanowires and silica nanoparticles as morphology controlled conductive filler applied in flexible conductive nanocomposites. *Compos Part A Appl S* 2015;73:195–203.
- [25] Wu C, Kim TW, Li F, Guo T. Wearable electricity generators fabricated utilizing transparent electronic textiles based on polyester/Ag nanowires/graphene core-shell nanocomposites. *ACS Nano* 2016;10(7):6449–57.
- [26] Amjadi M, Pichitpajongkit A, Lee S, Ryu S, Park I. Highly stretchable and sensitive strain sensor based on silver nanowire-elastomer nanocomposite. *ACS Nano* 2014;8(5):5154–63.
- [27] Lu N, Lu C, Yang S, Rogers J. Highly sensitive skin-mountable strain gauges based entirely on elastomers. *Adv Funct Mater* 2012;22(19):4044–50.
- [28] Xiao X, Yuan L, Zhong J, Ding T, Liu Y, Cai Z, et al. High-strain sensors based on zno nanowire/polystyrene hybridized flexible films. *Adv Mater* 2011;23(45):5440–4.
- [29] Park M, Park J, Jeong U. Design of conductive composite elastomers for stretchable electronics. *Nano Today* 2014;9(2):244–60.
- [30] Zeng W, Shu L, Li Q, Chen S, Wang F, Tao XM. Fiber-based wearable electronics: a review of materials, fabrication, devices, and applications. *Adv Mater* 2014;26(31):5310–36.
- [31] Stoppa M, Chiolerio A. Wearable electronics and smart textiles: a critical review. *Sensors* 2014;14(7):11957–92.
- [32] Lee S, Shin S, Lee S, Seo J, Lee J, Son S, et al. Ag nanowire reinforced highly stretchable conductive fibers for wearable electronics. *Adv Funct Mater* 2015;25(21):3114–21.
- [33] Fu KK, Cheng J, Li T, Hu L. Flexible batteries: from mechanics to devices. *ACS Energy Letters* 2016;1(5):1065–79.
- [34] Cheng Y, Zhang H, Wang R, Wang X, Zhai H, Wang T, et al. Highly stretchable and conductive copper nanowire based fibers with hierarchical structure for wearable heaters. *ACS Appl Mat Inter* 2016;8(48):32925–33.
- [35] Liao X, Liao Q, Zhang Z, Yan X, Liang Q, Wang Q, et al. A Highly stretchable ZnO@ fiber-based multifunctional nanosensor for strain/temperature/UV detection. *Adv Funct Mater* 2016.
- [36] Huang G, Liu L, Wang R, Zhang J, Sun X, Peng H. Smart color-changing textile with high contrast based on a single-sided conductive fabric. *J Mater Chem C* 2016;4(32):7589–94.
- [37] Lv T, Yao Y, Li N, Chen T. Wearable fiber-shaped energy conversion and storage devices based on aligned carbon nanotubes. *Nano Today* 2016;11(5):644–60.
- [38] Zhou H, Yan L, Jiang W, Xuan S, Gong X. Shear thickening fluid-based energy-free damper: design and dynamic characteristics. *J Intell Mater Syst Struct* 2016;27(2):208–20.
- [39] Ge L, Gong X, Wang Y, Xuan S. The conductive three dimensional topological structure enhanced magnetorheological elastomer towards a strain sensor. *Compos Sci Technol* 2016;135:92–9.
- [40] Yang C, Gu H, Lin W, Yuen MM, Wong CP, Xiong M, et al. Silver nanowires: from scalable synthesis to recyclable foldable electronics. *Adv Mater* 2011;23(27):3052–6.
- [41] Wang Y, Zhang X, Chung K, Liu C, Choi S-B, Choi HJ. Formation of core-shell structured complex microparticles during fabrication of magnetorheological elastomers and their magnetorheological behavior. *Smart Mater Struct* 2016;25(11):115028.
- [42] Qiao X, Lu X, Li W, Chen J, Gong X, Yang T, et al. Microstructure and magnetorheological properties of the thermoplastic magnetorheological elastomer composites containing modified carbonyl iron particles and poly(styrene-*b*-ethylene-ethylene-propylene-*b*-styrene) matrix. *Smart Mater Struct* 2012;21(11):115028.
- [43] Li J, Zhang M, Wang L, Li W, Sheng P, Wen W. Design and fabrication of microfluidic mixer from carbonyl iron-PDMS composite membrane. *Microfluid Nanofluid* 2011;10(4):919–25.
- [44] Imaduddin F, Li Y, Mazlan SA, Sutrisno J, Koga T, Yahya I, et al. A new class of magnetorheological elastomers based on waste tire rubber and the characterization of their properties. *Smart Mater Struct* 2016;25(11):115002.
- [45] Amjadi M, Kyung KU, Park I, Sitti M. Stretchable, skin-mountable, and wearable strain sensors and their potential applications: a review. *Adv Funct Mater* 2016.
- [46] Cheng B, Yuan L, Zhu W, Song Y, Xiao H. A coaxial cable magnetic field sensor based on ferrofluid filled Fabry-Perot interferometer structure. *Sensor Actuat A-Phys* 2017;257:194–7.
- [47] Luo L, Pu S, Tang J, Zeng X, Lahoubi M. Highly sensitive magnetic field sensor based on microfiber coupler with magnetic fluid. *Appl Phys Lett* 2015;106(19):193507.
- [48] Wang S, Jiang W, Jiang W, Ye F, Mao Y, Xuan S, et al. Multifunctional polymer composite with excellent shear stiffening performance and magnetorheological effect. *J Mater Chem C* 2014;2(34):7133–40.
- [49] Kwok SW, Morin SA, Mosadegh B, So JH, Shepherd RF, Martinez RV, et al. Magnetic assembly of soft robots with hard components. *Adv Funct Mater* 2014;24(15):2180–7.
- [50] Gong X, Yang K, Xie J, Wang Y, Kulkarni P, Hobbs AS, et al. Rotary actuators based on pneumatically driven elastomeric structures. *Adv Mater* 2016;28(34):7533–8.